# Photochemical conversion of AgCl nanocubes to hybrid AgCl–Ag nanoparticles with high activity and long-term stability towards photocatalytic degradation of organic dyes

**Jizhuang Wang, Changhua An, Meiyu Zhang, Chuan Qin, Xijuan Ming, and Qinhui Zhang**



**Abstract:** The performance of a photocatalytic reaction is mainly determined by the quality of the photocatalyst. For real applications, significantly enhancing the stability and activity of the photocatalysts still remains a challenge for materials scientists and chemists. In this paper, we have achieved a highly efficient plasmonic AgCl–Ag nanophotocatalyst via photochemical conversion of AgCl nanocubes. Compared with reported photocatalysts, the as-achieved nanophotocatalyst exhibits superior activity, long-term stability, and wide applicability in the decomposition of organic dye pollutants. For example, only 30 s is needed to bleach methyl orange molecules assisted by AgCl–Ag nanoparticles. Furthermore, the catalyst can be reused up to 50 times without significant loss of activity. A possible mechanism was discussed and the specified photocatalytic reactions verified that both $O_2^{\bullet-}$ and $OH^{\bullet}$ radicals were the main active species in decomposing pollutants. The excellent performance of the present photocatalyst suggests promising applications in environmental remediation, clean energy creation, and solar cells.

*Key words:* pasmonic photocatalyst, silver chloride, visible light photocatalysis, organic pollutant.

**Résumé :** La performance d'une réaction photocatalytique est déterminée principalement par la qualité du photocatalyseur. Pour des applications réelles, l'augmentation significative de la stabilité et de l'activité du photocatalyseur reste le défi à surmonter pour les scientifiques et les chimistes. Dans ce travail, on a préparé un nanophotocatalyseur AgCl–Ag plasmonique très efficace en procédant à une conversion photochimique de nanocubes de AgCl. Par comparaison avec les photocatalyseurs rapportés antérieurement, le nanophotocatalyseur tel que préparé présente une activité supérieure, une stabilité à long terme et une large plage de domaines d'application dans la décomposition des colorants organiques polluants. Par exemple, à l'aide de nanoparticules de AgCl–Ag, il suffit de 30 s pour blanchir des molécules de méthylorange. De plus, le catalyseur peut être réutilisé jusqu'à 50 fois sans perte significative d'activité. On discute d'un mécanisme potentiel pour cette réaction et, faisant appel à des radicaux $O_2^{\bullet-}$ et $OH^{\bullet}$, il a été possible de vérifier que les réactions photocatalytiques spécifiées sont bien les espèces catalytiques principales dans la décomposition des polluants. L'excellente performance de ce photocatalyseur suggère qu'il devrait posséder des applications prometteuses dans la dépollution environnementale, la création d'énergie propre et dans les cellules solaires.

*Mots-clés :* photocatalyseur plasmonique, chlorure d'argent, photocatalyseur à la lumière visible, polluant organique.

[Traduit par la Rédaction]

## Introduction

Since the discovery of photocatalytic splitting of water to produce hydrogen on $TiO_2$ electrodes,[1] photocatalysis has attracted much attention as a promising green approach for utilizing solar energy to solve energy and environmental issues. Great progress has been made in the fields of new energy generation,[2–4] conversion of carbon dioxide into valuable chemicals,[5–7] environmental purification,[8,9] solar cells,[10] and water disinfection.[11,12] Nowadays, the development of visible light driven photocatalysts has become one of the most important topics in this area. The strategies to create visible-light response photocatalysts can be classified into two categories. One is to narrow the band gap of $TiO_2$ by doping external elements, i.e., metals or nonmetals,[13–16] and engineering microstructures of titanate.[17] The other is to explore complex oxide visible photocatalysts, such as $Ag_3PO_4$,[18] $InTaO_4$,[2] $BiFeO_3$,[19,20] $Bi_2WO_6$,[21,22] and $PbBi_2Nb_2O_9$.[23] For real

Received 25 May 2012. Accepted 13 August 2012. Published at www.nrcresearchpress.com/cjc on 12 November 2012.

**J. Wang, C. An, M. Zhang, C. Qin, and X. Ming.** State Key Laboratory of Heavy Oil Processing and College of Science, China University of Petroleum, Qingdao, Shandong 266555, P.R. China.
**Q. Zhang.** State Key Laboratory of Heavy Oil Processing, College of Chemical Engineering, China University of Petroleum, Qingdao, Shandong 266555, P.R. China.

**Corresponding author:** Changhua An (e-mail: anchh@upc.edu.cn).

applications, significantly enhancing the stability and activity of the photocatalysts still remains a challenge to materials scientists and chemists.

Nanoparticles of noble metals, i.e., Au and Ag with surface plasmon resonance (SPR) effects, exhibit high absorption efficiency in the visible region, making them an ideal class of light absorber materials in the photocatalysis field.[24,25] Doping $TiO_2$ with Au (or Ag) has been demonstrated to greatly enhance the photoactivity of $TiO_2$ by reducing the recombination rate of the photogenerated charge carriers.[24,26–28] The absorption edges of $TiO_2$ were only extended to approximately 420 nm, leading to most of the solar spectrum being unable to drive these photocatalysts.

Silver halides decorated with Ag or Au represent a class of promising plasmonic photocatalysts because they not only exhibit high absorption coefficients in the visible region owing to the contribution of SPR, but also show enhanced photocatalytic performance.[29–31] For example, Ag@AgCl (or AgBr) photocatalysts have been prepared[29,32] through ion-exchange reactions followed by the UV conversion of some $Ag^+$ to $Ag^0$ on the surfaces of the parent crystallites. The microscale and irregular shapes of the obtained catalysts result in reduced surface areas, unclear interfaces, and thus reduced catalytic performance compared with nanoparticles. Therefore, creating photocatalysts with high activity, long-term stability, and wide applicability is of paramount importance and highly desirable.

Herein, we have developed a simple photochemical conversion of AgCl nanocubes to fabricate a class of long-term stable hybrid plasmonic AgCl–Ag nanoparticles with superior activity towards the decomposition of organic pollutants, i.e., methyl orange (MO), rhodamine B (RhB), methylene blue (MB), malachite green (MG), crystal violet (CV), alizarin red (AR), and methyl red (MR). MO molecules can be rapidly decomposed within 30 s under visible light irradiation with the assistance of the AgCl–Ag nanoparticles. The catalyst can be recycled up to 50 times without losing activity. These features mean the as-achieved nanophotocatalysts have good prospects in water disinfection and environmental remediation.

## Experimental

### Preparation of catalysts

AgCl nanocubes were synthesized by a simple polyol precipitation process.[30] In a typical procedure, 10 mL of ethylene glycol (EG, Sinopharm Chemical Reagent Co., Ltd) was placed in a 50 mL flask and heated at 60 °C under magnetic stirring at 350 rpm. Then poly(vinyl pyrrolidone) (PVP, 54 mg, Sinopharm Chemical Reagent Co., Ltd) and NaCl (22 mg, AR, Sinopharm Chemical Reagent Co., Ltd) were added. After they were dissolved completely, a 1 mL EG solution of $AgNO_3$ (52 mg/mL, Sinopharm Chemical Reagent Co., Ltd) was rapidly injected to this mixture. The mixture was maintained at 60 °C for 30 min, resulting in a milky dispersion containing AgCl nanoparticles. The sample was rinsed with deionized water several times and collected via centrifugation.

The as-prepared AgCl nanoparticles can be easily dispersed in 10 mL deionized water. The water dispersion of AgCl was irradiated with a 300 W Xe arc lamp equipped with an UV cutoff filter for different times, i.e., 0, 20, 40, and 60 min (corresponding samples were denoted as AgCl, AgCl–Ag-20, AgCl–Ag-40, AgCl–Ag-60, respectively). The color of the resulting dispersion changed from milky to grayish purple, indicating metallic silver nanoparticles were produced on the surfaces of AgCl. The synthesis of the referred catalyst (AgCl–Ag-ref) is described in the Supplementary data.

**Fig. 1.** X-ray diffraction (XRD) pattern of the as-prepared AgCl–Ag nanoparticles.

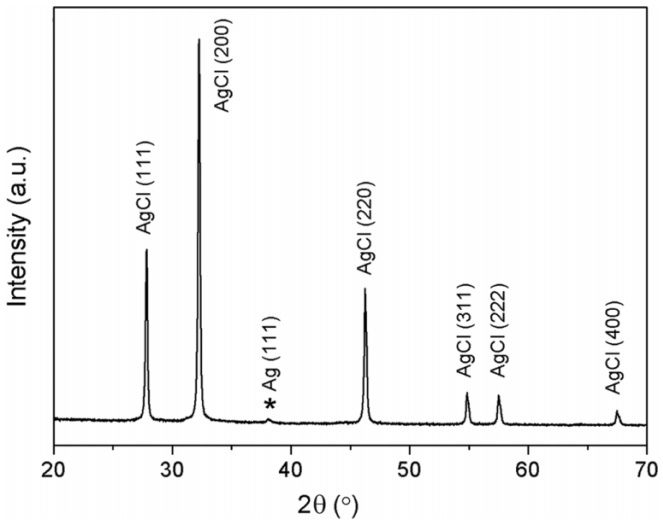


### Characterization

The crystalline phases of the products were analyzed by X-ray diffraction (XRD, Philips X'Pert with Cu Kα radiation (λ = 0.154 18 nm). The morphology and size of the AgCl–Ag nanoparticles were observed by an S-4800 field emission scanning electron microscope (SEM; Hitachi, Japan). The optical absorption spectra were measured on a UV–vis spectrometer (Specord 205, Analytik Jena) over a range of 200 to 900 nm.

### Evaluation of photocatalytic performance

In a typical reaction, a 10 mL water dispersion of the as-prepared AgCl–Ag nanoparticles was transferred to an aqueous solution of MO (10 mL, 10 mg $L^{-1}$). The mixture was stored in the dark for 60 min with magnetic stirring to reach the adsorption–desorption equilibrium of MO molecules on the surface of the nanoparticles. The reaction was then started under a 300 W Xe arc lamp (PLS-SXE300/300UV) equipped with a UV cutoff filter as the visible light source (λ ≥ 400 nm). The degradation rate of MO was measured by UV–vis spectroscopy at different times. After the reaction was completed, centrifuging the solution enables the AgCl–Ag nanoparticles to be collected to catalyze new reactions.

For the degradation of RhB, MB, MG, CV, and alAR, the conditions were kept identical to that of MO except that half the amount of the as-prepared AgCl–Ag nanoparticles was used. The decomposition of MR was performed in ethanol solution because of its insolublity in water.

## Results and discussion

### Characterization of the AgCl–Ag photocatalyst

Figure 1 presents an XRD pattern of the as-prepared AgCl–Ag nanoparticles. It clearly shows that the sample is composed of cubic AgCl (JCPDS card No. 31-1238) and metallic Ag (JCPDS card No. 87-0717). The diffraction peaks at 27.28°, 32.23°, 46.24°, 54.82°, 57.49°, and 67.46° can be

**Fig. 2.** X-ray photoelectron spectroscopy (XPS) spectra of the as-prepared AgCl–Ag. (A) survey, (B) Ag 3d, and (C) Cl 2p.

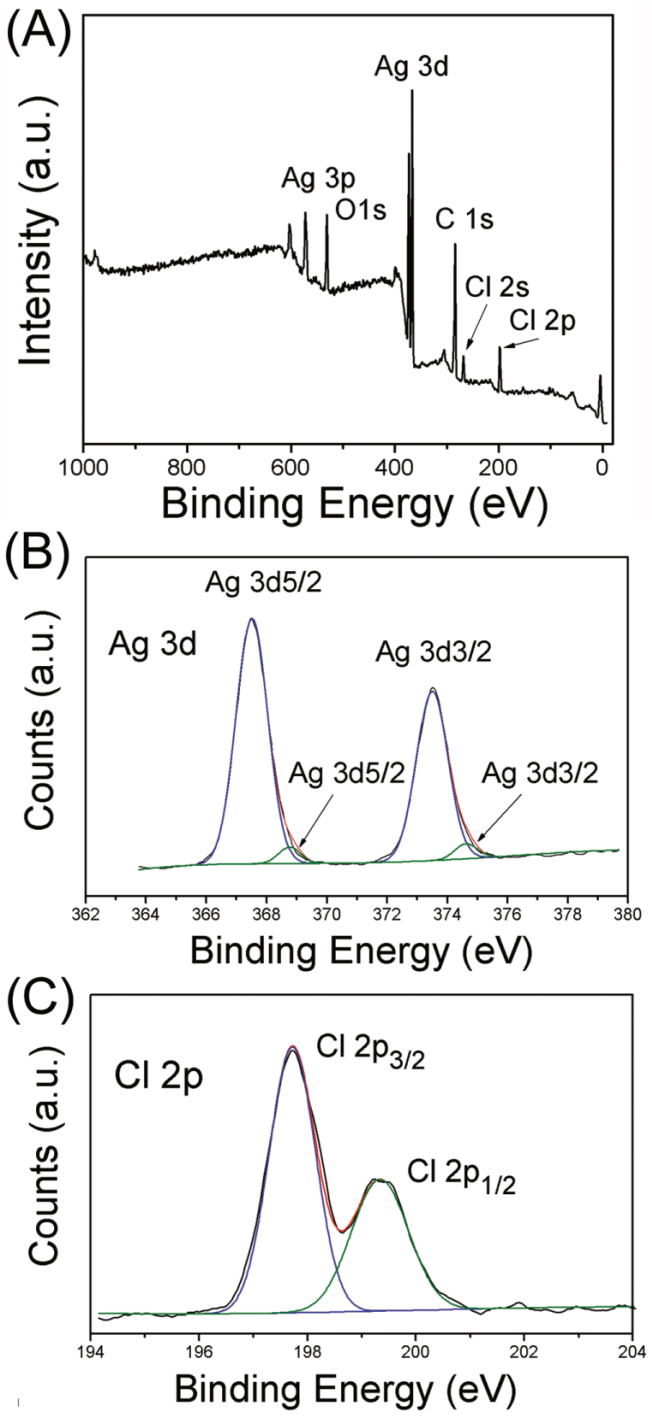


**Fig. 3.** (A) SEM images of AgCl–Ag. The inset at the top right corner shows the AgCl nanoparticles (scale bar is the same as for AgCl–Ag). (B) UV–vis absorbance spectra of AgCl and AgCl–Ag.

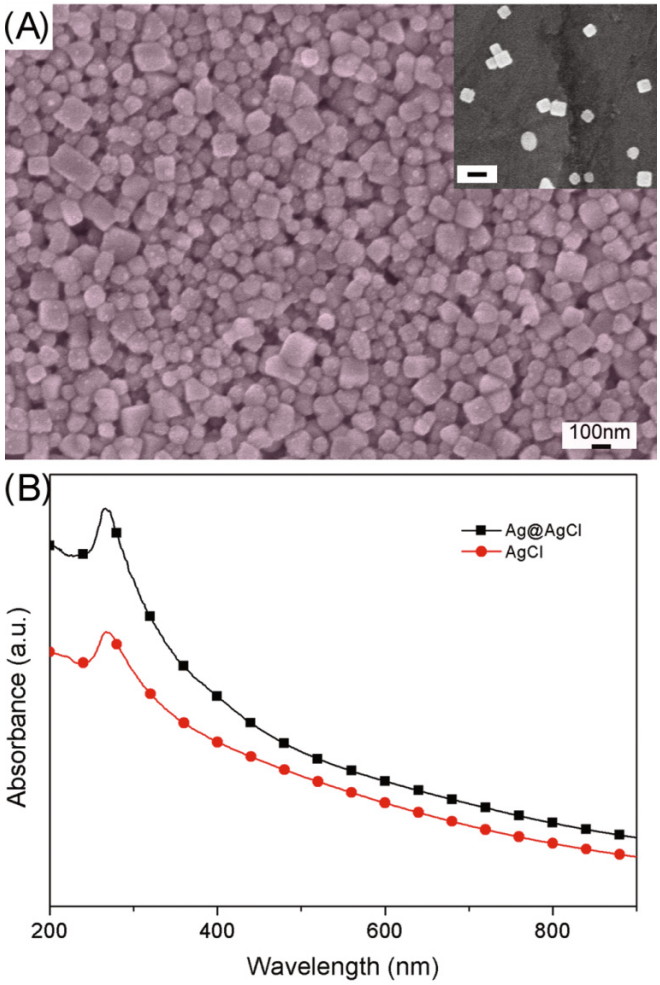


assigned to the (111), (200), (220), (311), (222), and (400) planes, respectively, of the AgCl nanoparticles. The peak at 38.07° is attributed to the diffraction of the (111) plane of metallic Ag. The elemental composition and silver content of the AgCl–Ag were further confirmed by X-ray photoelectron spectroscopy (XPS). Figure 2A reveals that Ag and Cl are the main components, and trace amounts of C and O are the adventitious hydrocarbon from the XPS instrument. As shown in Fig. 2B, the peaks at 367.5 and 373.5 eV may be assigned to the binding energy of Ag 3d 5/2 and Ag 3d 3/2 of $Ag^+$ in AgCl, respectively, and the peaks at 368.8 and 374.6 eV may be attributed to metallic $Ag^0$. The results confirmed the existence of $Ag^0$, and the surface ratio of metallic $Ag^0$ and $Ag^+$ is approximately 1:13. For Cl 2p, two peaks are observed at the binding energies of 197.7 and 199.3 eV.

Figure 3A shows the SEM images of as-prepared AgCl (inset) and AgCl–Ag nanoparticles. The smooth AgCl nanoparticles exhibit a cubic shape with an average edge length of 90 nm. After photochemical reduction, Ag nanoparticles are assembled on the surfaces of the parent AgCl nanocubes. The AgCl–Ag hybrid nanoparticles display convex a cubic and near-spherical shape. The UV–vis absorption spectra (Fig. 3B) of the parent AgCl and AgCl–Ag nanoparticles exhibit a similar shape, indicating that tiny Ag nanoparticles are distributed evenly on the surfaces of AgCl nanocubes. For AgCl, there is little absorption in the visible region due to its large band gaps, i.e., a direct band gap of 5.15 eV (241 nm) and an indirect band gap of 3.25 eV (382 nm).[33] The AgCl–Ag

**Fig. 4.** (A) The change in UV–vis spectra for the methyl orange (MO) solution with reaction time. (B) The normalized concentration of the MO as a function of reaction time in both linear (–■–) and logarithmic (–●–) scale. $C_0$ is the concentration of MO before irradiation; $C$ is the concentration of MO at reaction time $t$.

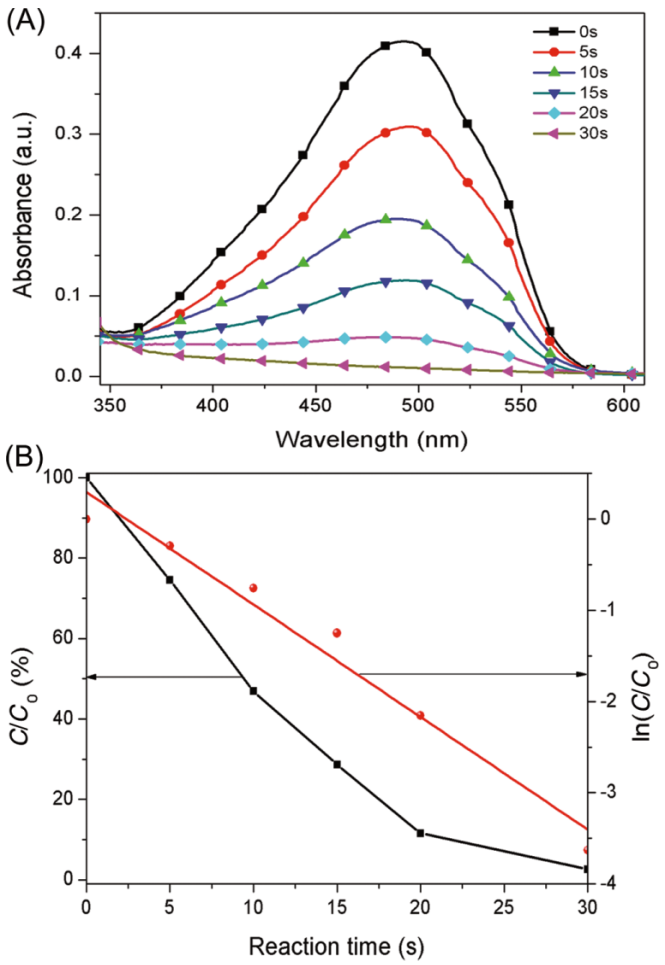


nanoparticles show a stronger absorption in the visible region than the parent AgCl owing to the SPR of the Ag species.

## Photocatalytic performance of AgCl–Ag

The photocatalytic performance of the as-prepared AgCl–Ag nanoparticles was evaluated by degradation of MO (5 mg $L^{-1}$) molecules under visible light irradiation. Figure 5A shows the evolution of the absorption spectra of methyl orange (MO) with reaction time over the AgCl–Ag-20 nanophotocatalyst. The color of the MO solution gradually changes from orange to transparent as the reaction proceeds (Supplementary data, Fig. S1), and the MO molecules rapidly decomposed within 30 s under visible light irradiation with the assistance of the AgCl–Ag nanoparticles. The blank tests in the dark with AgCl, AgCl–Ag, and under visible light without catalyst were carried out. The color of the MO solution remained unchanged, demonstrating that the AgCl–Ag nanoparticles are crucial for the degradation of the dye. Meanwhile, the effects of Ag on the photocatalytic activity were also investigated by a series of controlled experiments. As shown in Fig. 5, AgCl–Ag-20 shows the best photocatalytic performance compared with the

**Fig. 5.** Photocatalytic degradation of methyl orange (MO) for different samples under visible light irradiation, showing that AgCl–Ag-20 nanoparticles exhibits the highest performance. AgCl–Ag-20, AgCl irradiated with a 300 W Xe arc lamp for 20 min.

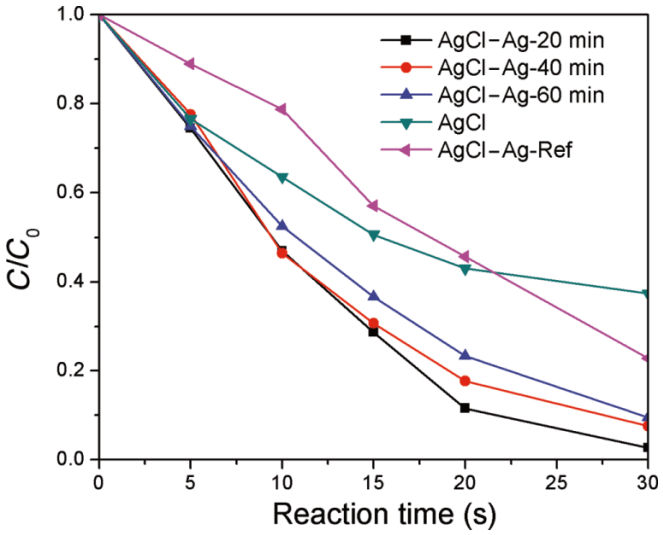


**Fig. 6.** The degradation curve of methyl orange (MO) solution for 50 successive reactions catalyzed with the same batch of AgCl–Ag-20 nanoparticles (as shown in Fig. 1) under visible light irradiation. AgCl–Ag-20, AgCl irradiated with a 300 W Xe arc lamp for 20 min.

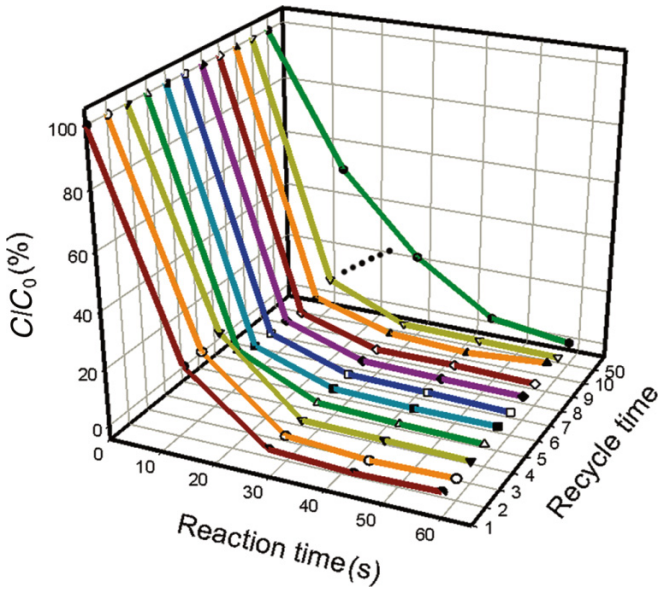


other samples. However, AgCl–Ag-20 also shows higher activity than pure AgCl, which only degrades 63% of MO within the same time frame. The enhanced activity of AgCl–Ag may account for the synergy between the SPRs of Ag nanograins on the surface of AgCl and the polarization field from AgCl. Furthermore, the Brunauer–Emmett–Teller (BET) nitrogen adsorption analysis reveals that the specific surface area was 33.2 $m^2$ $g^{-1}$, further suggesting that the enhanced activity is not caused merely by its surface property. While excessive Ag may increase the probability of hole capture by the negative

**Fig. 7.** Schematic illustration of the photocatalytic reaction pathway of AgCl–Ag nanoparticles under visible light.

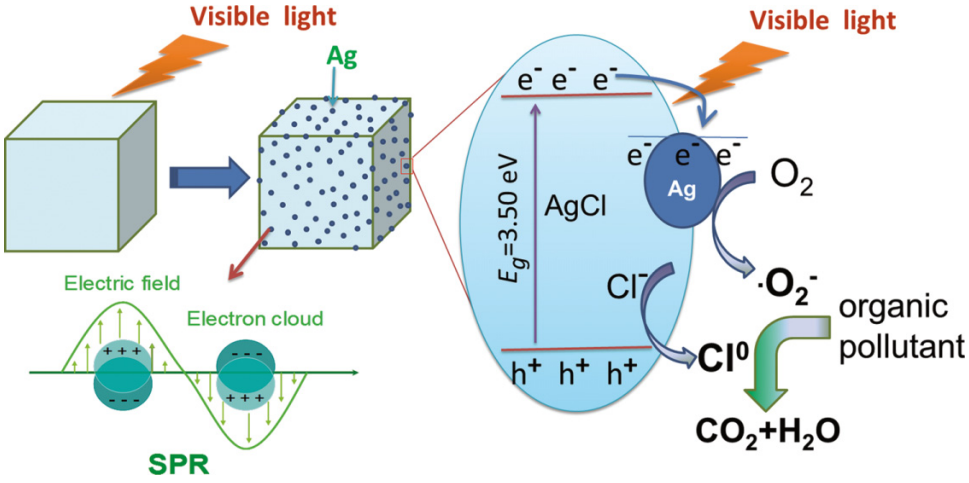


charge on the Ag nanoparticles, and destroy the structure of the as-achieved catalyst, this may lead to the decreased activity of the catalysts containing a high content of Ag. The function of $\ln(C/C_0)$ versus reaction time ($t$; Fig. 4B) exhibits a linear relationship, indicating the reaction follows pseudo-first-order kinetics. The rate constant was determined to be 0.123 $s^{-1}$.

In consideration of practical applications, we also tested the stability and applicability of the present hybrid nanophotocatalyst. Figure 6 shows the recycled reactions using the same batch of catalysts. The used nanophotocatalyst can still maintain high efficiency even after 50 reactions. Note that if the dye concentration was increased to 10 mg $L^{-1}$, the catalyst can still be reused 35 times without much decrease in activity (Supplementary data Figs. S2 and S3). Inspired by the superior stability and activity of the photocatalysts, other typical organic pollutants, such as RhB, MB, MB, CV, AR, and MR, were also selected to trigger the degradation reactions. The results demonstrate that these dyes can also be bleached steadily (Supplementary data Fig. S4), confirming the broad applicability of the as-prepared AgCl–Ag nanophotocatalysts.

## Photocatalytic mechanism

Usually, semiconductor photocatalysts, e.g., $TiO_2$, have wide band gaps, which make them stable against corrosion in surrounding environments.[34,35] The band gap of the as-prepared AgCl nanocubes was determined to be 3.50 eV on the basis of UV–vis absorption spectrum (Supplementary data Fig. S5), which makes it a class of alternative stable photocatalysts, although visible-light excitation is difficult. The position of the conduction band ($E_{CB}$) of the AgCl nanocubes can be determined by the equation $E_{CB} = X - E_C - 0.5E_g$,[36] where $E_C$ represents the energy of the free electrons on the hydrogen scale (4.5 eV), $X$ is the electronegativity of the semiconductor, and $E_g$ represents the band gap of the semiconductor. Thus, the $E_{CB}$ and the position of the valence band ($E_{VB}$) were calculated to be −0.341 and 3.159 eV, respectively. As presented in Fig. 7A, a possible mechanism is proposed. Here, well-defined interfaces in hybrid AgCl–Ag nanoparticles may provide proper environments for enhancement of their photocatalytic performance. Ag nanoparticles can act as a sinker for photoinduced charge carriers, promoting charge separation to enhance the overall photocatalytic efficiency in contact with the parent semiconductor.[37,38] As reported by Huang and co-workers[29] and our group,[30] the interactions between the SPR of the Ag nanoparticles and the polarization field provided by the AgCl determine the photocatalytic efficiency. In the present system, photoillumination of uniform parent AgCl nanocubes results in an even distribution of Ag nanoparticles on their surfaces, and thus leads to more even charge distributions of the free electrons in Ag nanoparticles more evenly than previously reported.[29–32] In other words, regions of negative and positive charges in the Ag nanoparticles have been separated effectively, which are far from and close to the AgCl–Ag interface, respectively. The migration of photoexcited electrons away from the AgCl–Ag interfaces also prevents photoreduction of AgCl to Ag, leading to a high stability of the hybrid nanoparticles. Therefore, there is synergy between the enhanced absorption of visible light by the SPR of the Ag nanoparticles and the polarization field provided by the AgCl facilitates electron–hole separation and interfacial charge transfer. That is to say, electron and hole were delivered into the two distinct regions (Ag and AgCl region). In the Ag/solution region, photogenerated electrons can be scavenged by $O_2$ in the solution to form $O_2^{\bullet-}$ and other reactive oxygen species.[38–41] To confirm the roles of oxidizing species, radical and hole trapping tests weren designed to further elucidate the photocatalytic mechanism. As shown in Fig. 8, the $NaHCO_3$ scavenger for holes ($h^+$) and adsorbed $OH^{\bullet}$ have no significant effects on the activity of the catalyst. However, if 0.1 mol/L of *tert*-butyl alcohol for $OH^{\bullet}$ was introduced, the MO degradation rate was decreased (i.e., after reacting for 20 s, 46% MO was left in the solution.). With the addition of $O_2^{\bullet-}$ scavenger (*p*-benzoquinone), the rate of bleaching MO was depressed significantly. These results indicate that the surface-adsorbed $O_2^{\bullet-}$ and $OH^{\bullet}$ are active species in the reaction. Due to the longer life time of active $e^-$ compared with $h^+$,[39] the $O_2^{\bullet-}$ and $OH^{\bullet}$ generation can be produced by the following reactions

$$O_2 + e^- \rightarrow O_2^{\bullet-}$$

**Fig. 8.** Photodegradation kinetics of methyl orange (MO) in AgCl–Ag water dispersion under visible light irradiation with different scavengers.

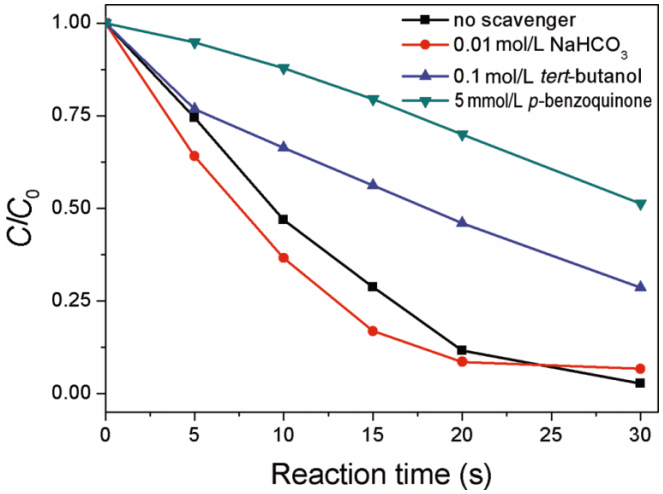


$$O_2^{\bullet -} + h^+ \rightarrow OOH^{\bullet}$$

$$OOH^{\bullet} + H^+ + e^- \rightarrow H_2O_2$$

$$H_2O_2 + e^- \rightarrow OH^{\bullet} + OH$$

Therefore, $O_2^{\bullet -}$ and $OH^{\bullet}$ radicals come from photoexcited electrons and accumulate on the silver surfaces, which is in accord with the previous discussion. Holes ($h^+$) play a minor role in the present reactions. The mechanism can be understood as a plasmon-induced photocatalytic reaction. Of course, further studies are still necessary to provide insight into the unraveling of the process of charge generation, transport, and the photocatalytic reaction mechanism.

## Conclusion

In summary, photochemical conversion of AgCl nanocubes has been demonstrated to be a facile strategy for the preparation of highly efficient plasmonic AgCl–Ag nanophotocatalysts with strong activity, stability, and wide applicability towards the decomposition of various organic dye pollutants. MO molecules can be decomposed completely within 30 s in the presence of the as-achieved nanophotocatalyst. Furthermore, it can be reused approximately 50 times without losing activity. The possible photocatalytic reaction mechanism indicates that Ag nanoparticles play an important role in enhancing the absorption of visible light, separating electron–hole pairs and generating oxidizing species. The excellent efficiency of the plasmonic nanophotocatalyst has promise for applications in environmental remediation, clean energy creation, and solar cells.

## Supplementary data

Supplementary data are available with the article throught the journal Web site at http://nrcresearchpress.com/doi/suppl/10.1139/v2012-079.



## Acknowledgement

This work was financially supported by the National Natural Science Foundation of China (Grant No. 21001116).

## References

(1) Fujishima, A.; Honda, K. *Nature* **1972**, *238* (5358), 37. doi:10.1038/238037a0.
(2) Zou, Z.; Ye, J.; Sayama, K.; Arakawa, H. *Nature* **2001**, *414* (6864), 625. doi:10.1038/414625a.
(3) Maeda, K.; Xiong, A.; Yoshinaga, T.; Ikeda, T.; Sakamoto, N.; Hisatomi, T.; Takashima, M.; Lu, D.; Kanehara, M.; Setoyama, T.; Teranishi, T.; Domen, K. *Angew. Chem. Int. Ed.* **2010**, *49* (24), 4096. doi:10.1002/anie.201001259.
(4) Ingram, D. B.; Linic, S. *J. Am. Chem. Soc.* **2011**, *133* (14), 5202. doi:10.1021/ja200086g.
(5) Liu, Q.; Zhou, Y.; Kou, J.; Chen, X.; Tian, Z.; Gao, J.; Yan, S.; Zou, Z. *J. Am. Chem. Soc.* **2010**, *132* (41), 14385. doi:10.1021/ja1068596.
(6) Roy, S. C.; Varghese, O. K.; Paulose, M.; Grimes, C. A. *ACS Nano* **2010**, *4* (3), 1259. doi:10.1021/nn9015423.
(7) Yokoi, N.; Miura, Y.; Huang, C.-Y.; Takatani, N.; Inaba, H.; Koshiyama, T.; Kanamaru, S.; Arisaka, F.; Watanabe, Y.; Kitagawa, S.; Ueno, T. *Chem. Commun. (Camb.)* **2011**, *47* (7), 2074. doi:10.1039/c0cc03015e.
(8) Chen, C.; Ma, W.; Zhao, J. *Chem. Soc. Rev.* **2010**, *39* (11), 4206. doi:10.1039/b921692h.
(9) Takahashi, D.; Hirono, S.; Hayashi, C.; Igarashi, M.; Nishimura, Y.; Toshima, K. *Angew. Chem. Int. Ed.* **2010**, *49* (52), 10096. doi:10.1002/anie.201005161.
(10) Kang, T. S.; Smith, A. P.; Taylor, B. E.; Durstock, M. F. *Nano Lett.* **2009**, *9* (2), 601. doi:10.1021/nl802818d.
(11) Chorianopoulos, N. G.; Tsoukleris, D. S.; Panagou, E. Z.; Falaras, P.; Nychas, G.-J. E. *Int. J. Food Microbiol.* **2011**, *28* (1), 164. doi:10.1016/j.fm.2010.07.025.
(12) Zhang, L.; Wong, K.-H.; Yip, H.-Y.; Hu, C.; Yu, J. C.; Chan, C.-Y.; Wong, P.-K. *Environ. Sci. Technol.* **2010**, *44* (4), 1392. doi:10.1021/es903087w.
(13) Kaden, W. E.; Wu, T.; Kunkel, W. A.; Anderson, S. L. *Science* **2009**, *326* (5954), 826. doi:10.1126/science.1180297.
(14) Jaimy, K. B.; Ghosh, S.; Sankar, S.; Warrier, K. G. K. *Mater. Res. Bull.* **2011**, *46* (6), 914. doi:10.1016/j.materresbull.2011.02.030.
(15) Khan, S. U. M. *Science* **2002**, *297* (5590), 2243. doi:10.1126/science.1075035.
(16) Chen, X.; Burda, C. *J. Am. Chem. Soc.* **2008**, *130* (15), 5018. doi:10.1021/ja711023z.
(17) Chen, X.; Liu, L.; Yu, P. Y.; Mao, S. S. *Science* **2011**, *331* (6018), 746. doi:10.1126/science.1200448.
(18) Yi, Z.; Ye, J.; Kikugawa, N.; Kako, T.; Ouyang, S.; Stuart-Williams, H.; Yang, H.; Cao, J.; Luo, W.; Li, Z.; Liu, Y.; Withers, R. L. *Nat. Mater.* **2010**, *9* (7), 559. doi:10.1038/nmat2780.
(19) Luo, J.; Maggard, P. A. *Adv. Mater. (Deerfield Beach Fla.)* **2006**, *18* (4), 514. doi:10.1002/adma.200500109.
(20) Gao, F.; Chen, X. Y.; Yin, K. B.; Dong, S.; Ren, Z. F.; Yuan, F.; Yu, T.; Zou, Z. G.; Liu, J.-M. *Adv. Mater. (Deerfield Beach Fla.)* **2007**, *19* (19), 2889. doi:10.1002/adma.200602377.
(21) Zhang, L. W.; Wang, Y.-J.; Cheng, H.-Y.; Yao, W.-Q.; Zhu, Y.-F. *Adv. Mater. (Deerfield Beach Fla.)* **2009**, *21* (12), 1286. doi:10.1002/adma.200801354.

(22) Fu, H.; Pan, C.; Zhang, L.; Zhu, Y. *Mater. Res. Bull.* **2007**, *42* (4), 696. doi:10.1016/j.materresbull.2006.07.017.
(23) Kim, H. G.; Hwang, D. W.; Lee, J. S. *J. Am. Chem. Soc.* **2004**, *126* (29), 8912. doi:10.1021/ja049676a.
(24) Awazu, K.; Fujimaki, M.; Rockstuhl, C.; Tominaga, J.; Murakami, H.; Ohki, Y.; Yoshida, N.; Watanabe, T. *J. Am. Chem. Soc.* **2008**, *130* (5), 1676. doi:10.1021/ja076503n.
(25) Zhang, Q.; Ge, J.; Pham, T.; Goebl, J.; Hu, Y.; Lu, Z.; Yin, Y. *Angew. Chem. Int. Ed.* **2009**, *48* (19), 3516. doi:10.1002/anie.200900545.
(26) Tian, Y.; Tatsuma, T. *J. Am. Chem. Soc.* **2005**, *127* (20), 7632. doi:10.1021/ja042192u.
(27) Subramanian, V.; Wolf, E. E.; Kamat, P. V. *J. Am. Chem. Soc.* **2004**, *126* (15), 4943. doi:10.1021/ja0315199.
(28) Hou, W.; Liu, Z.; Pavaskar, P.; Hung, W. H.; Cronin, S. B. *J. Catal.* **2011**, *277* (2), 149. doi:10.1016/j.jcat.2010.11.001.
(29) Wang, P.; Huang, B.; Qin, X.; Zhang, X.; Dai, Y.; Wei, J.; Whangbo, M.-H. *Angew. Chem. Int. Ed.* **2008**, *47* (41), 7931. doi:10.1002/anie.200802483.
(30) An, C.; Peng, S.; Sun, Y. *Adv. Mater. (Deerfield Beach Fla.)* **2010**, *22* (23), 2570. doi:10.1002/adma.200904116.
(31) Hu, C.; Peng, T.; Hu, X.; Nie, Y.; Zhou, X.; Qu, J.; He, H. *J. Am. Chem. Soc.* **2010**, *132* (2), 857. doi:10.1021/ja907792d.
(32) Wang, P.; Huang, B.; Zhang, X.; Qin, X.; Jin, H.; Dai, Y.; Wang, Z.; Wei, J.; Zhan, J.; Wang, S.; Wang, J.; Whangbo, M.-H. *Chem. Eur. J.* **2009**, *15* (8), 1821. doi:10.1002/chem.200802327.
(33) Glaus, S.; Calzaferri, G. *Photochem. Photobiol.* **2003**, *2* (4), 398. doi:10.1039/b211678b.
(34) Albu, S. P.; Ghicov, A.; Macak, J. M.; Hahn, R.; Schmuki, P. *Nano Lett.* **2007**, *7* (5), 1286. doi:10.1021/nl070264k.
(35) Varghese, O. K.; Gong, D.; Paulose, M.; Ong, K. G.; Dickey, E. C.; Grimes, C. A. *Adv. Mater. (Deerfield Beach Fla.)* **2003**, *15* (78), 624. doi:10.1002/adma.200304586.
(36) Liu, Q.; Zhou, Y.; Kou, J.; Chen, X.; Tian, Z.; Gao, J.; Yan, S.; Zou, Z. *J. Am. Chem. Soc.* **2010**, *132* (41), 14385. doi:10.1021/ja1068596.
(37) Hirakawa, T.; Kamat, P. V. *J. Am. Chem. Soc.* **2005**, *127* (11), 3928. doi:10.1021/ja042925a.
(38) Choi, M.; Shin, K.-H.; Jang, J. *J. Colloid Interface Sci.* **2010**, *341* (1), 83. doi:10.1016/j.jcis.2009.09.037.
(39) Hoffmann, M. R.; Martin, S. T.; Choi, W.; Bahnemann, D. W. *Chem. Rev.* **1995**, *95* (1), 69. doi:10.1021/cr00033a004.
(40) Houas, A. *Appl. Catal. B* **2001**, *31* (2), 145. doi:10.1016/S0926-3373(00)00276-9.
(41) Soni, S. S.; Henderson, M. J.; Bardeau, J.-F.; Gibaud, A. *Adv. Mater. (Deerfield Beach Fla.)* **2008**, *20* (8), 1493. doi:10.1002/adma.200701066.